

Enhancement of mechanical properties of biocompatible Ti–45Nb alloy by hydrostatic extrusion

K. Ozaltin · W. Chrominski · M. Kulczyk ·
A. Panigrahi · J. Horky · M. Zehetbauer ·
M. Lewandowska

Received: 30 March 2014 / Accepted: 10 June 2014 / Published online: 1 July 2014
© The Author(s) 2014. This article is published with open access at Springerlink.com

Abstract β -Type titanium alloys are promising materials for orthopaedic implants due to their relatively low Young's modulus and excellent biocompatibility. However, their strength is lower than those of α - or $\alpha + \beta$ -type titanium alloys. Grain refinement by severe plastic deformation (SPD) techniques provides a unique opportunity to enhance mechanical properties to prolong the lifetime of orthopaedic implants without changing their chemical composition. In this study, β -type Ti–45Nb (wt%) biomedical alloy in the form of 30 mm rod was subjected to hydrostatic extrusion (HE) to refine the microstructure and improve its mechanical properties. HE processing was carried out at room temperature without intermediate annealing in a multi-step process, up to an accumulative true strain of 3.5. Significant microstructure refinement from a coarse-grained region to an ultrafine-grained one was observed by optical and transmission electron microscopy. Vickers hardness measurements ($HV_{0.2}$) demonstrated that the strength of the alloy increased from about 150 to 210 $HV_{0.2}$. Nevertheless, the measurements of Young's modulus by nanoindentation showed no significant changes. This finding is substantiated by X-ray diffraction analyses which did not exhibit any phase

transformation out of the bcc phase being present still before processing by HE. These results thus indicate that HE is a promising SPD method to obtain significant grain refinement and enhance strength of β -type Ti–45Nb alloy without changing its low Young's modulus, being one prerequisite for biomedical application.

Introduction

Pure titanium and its alloys are frequently used in biomedical applications as implants due to their excellent mechanical properties, high corrosion resistance [1–4] and better strength/weight ratio compared to other metallic materials [5, 6]. Apart from mechanical properties, they also exhibit good biocompatibility, which is an essential requirement to avoid inflammation and long-term diseases [7].

α -Type commercially pure titanium (CP-Ti) and $\alpha + \beta$ -type Ti–6Al–4 V are well-known biomaterials which are commonly used as orthopaedic implants so far [4, 8]. However, their Young's modulus of about 100–110 GPa [1] is well above the Young's modulus of bones (10–30 GPa) [1, 9, 10]. This mismatch might cause absorption of bone and premature failure of the implant during utilization as a result of stress shielding effect [1, 2, 10, 11]. In addition, Ti–6Al–4 V alloy contains toxic elements such as Al, which causes neurological diseases like Alzheimer, Osteomalacia and metabolic bone diseases [12], and V which is incompatible with tissue in animals [5]. On the other hand, β -type titanium alloys are promising biometallic materials since they usually contain non-toxic elements and exhibit relatively low Young's modulus compared to α - and $\alpha + \beta$ -type alloys [2, 13].

Among β -type titanium alloys, Ti–Nb binary alloys consisting of 40–45 wt% of β -stabilizer non-toxic [13] and

K. Ozaltin (✉) · W. Chrominski · M. Lewandowska
Faculty of Materials Science and Engineering, Warsaw
University of Technology, Woloska 141, 02-507 Warsaw,
Poland
e-mail: kadir.ozaltin@inmat.pw.edu.pl

M. Kulczyk
Institute of High Pressure Physics, Polish Academy of Sciences,
Sokolowska 29/37, 01-142 Warsaw, Poland

A. Panigrahi · J. Horky · M. Zehetbauer
Physics of Nanostructured Materials, Faculty of Physics,
University of Vienna, Boltzmannngasse 5, 1090 Vienna, Austria

non-allergic [14] niobium are attractive orthopaedic materials due to their lowest Young's modulus of ~ 62 GPa [2, 8]. On the other hand, mechanical strength of β -type alloys is significantly lower than those of CP-Ti and Ti–6Al–4 V. Enhancement in mechanical properties to prolong the lifetime of the implant without alloying is possible by severe plastic deformation (SPD) [4, 15, 16]. In recent years, a number of SPD techniques have been developed, including equal-channel angular extrusion (ECAP) [17, 18], high-pressure torsion (HPT) [10, 19], accumulative roll bonding (ARB) [20] and hydrostatic extrusion (HE) [21, 22]. They bring about grain refinement down to sub-micron scale [21]. The characteristic features of SPD materials include deformation-induced high-angle grain boundaries [23] and high dislocation density inside the grains [24]. Also, the reduction of grain size contributes to enhancement of both the strength and the fatigue limit [25], which is quantitatively described by the Hall–Petch relationship [26, 27].

It has been demonstrated that HE is an efficient method to reduce the grain size in metallic materials [28, 29]. The grain size depends on the material being processed and process condition, e.g. accumulated strain. The typical grain size ranges from 500 nm for pure Al, 60 nm for a 7475 Al alloy and 50 nm for CP-Ti [21, 28, 30–32]. In this paper, we report recent results on microstructure and mechanical properties of β -type Ti–45Nb biomedical titanium alloy processed by hydrostatic extrusion.

Experimental

The material studied was a β -type Ti–45Nb (wt%) alloy with chemical composition given in Table 1.

Ti–45Nb alloy was supplied in the form of hot-extruded bar, 42 mm in diameter, featuring an average grain size of 23 μm , hereafter denoted as coarse-grained (CG) sample. HE was performed at room temperature (293 K) in a multi-step process (six passes). The initial diameter was 30 mm, whereas the final one was 5 mm, which correspond to a total true strain of 3.5 (the true strain is calculated by $\varepsilon = 2\ln(d_i/d_f)$, where d_i is the initial and d_f is the final diameter, respectively). The direction of the HE was parallel to the longitudinal direction of the bar and the measured hydrostatic pressure was about 1 GPa during each

pass. The parameters of all stages of HE are summarized in Table 2. HE-processed samples are denoted HEx, where x stands for sample's diameter.

The microstructure was observed using optical and transmission electron microscope (TEM) Jeol JEM 1200 (operated at 120 kV). All TEM samples were prepared from transverse sections of the specimens. The revealed microstructures were quantitatively described in terms of grain size using equivalent diameter d_2 , which is defined as the diameter of a circle which has the same surface area as the measured grains. Phase characterizations were carried out by X-ray diffraction (XRD) analysis (AXS Bruker D8 diffractometer) using a Cu K_α radiation ($\lambda = 0.154$ nm) with 0.8 mm spot size for transverse sections of all samples after mirror-like polishing.

Microhardness tests were performed using a Zwick Roell ZHU 2.5 testing facility by means of Vickers hardness. All indentations were carried out using a load of 200 g ($\text{HV}_{0.2}$) for ten measurements on transverse section of each specimen. Then, the average value and the standard deviation were calculated (see Fig. 1). Micro-tensile specimens were prepared in dumbbell-shaped form by spark erosion machine along the extrusion direction with a total length of 8 mm, 0.75 mm width, and 0.45 mm thickness with the parallel gauge length of 2.5 mm. Tensile tests were carried out for CG and HE5 samples at room temperature with constant crosshead speed and initial strain rate of 10^{-3} s $^{-1}$ (see Fig. 2).

Nanoindentation measurements were carried out with a load rate of 100 mN/20 s using a Vickers indenter (creep at 100 mN for 30 s and thermal drift at 10 mN for 60 s) to reveal changes in Young's modulus. The method of Oliver and Pharr [33] was used to determine the Young's modulus from load–displacement curves (the Poisson's ratio was assumed to be 0.41). Twenty-five indentations have been applied per specimen. The average values of Young's modulus as well as of standard deviation were calculated (see Fig. 3).

Results and discussion

HE processing induces a significant increase in the microhardness, as illustrated in Fig. 1. The most pronounced hardening is observed for the low values of applied strain; then the microhardness tends to stabilize and shows even a decrease for the highest applied strain. Especially the latter can be attributed to recovery and recrystallization processes, which are likely to take place during subsequent passes of HE [32], and also occur in other SPD techniques as cold rolling [34] and HPT [35, 36], respectively. In general, the microhardness increased from 149 $\text{HV}_{0.2}$ for CG sample to 195 $\text{HV}_{0.2}$ obtained for HE7 sample (which corresponds to a true strain of 2.83).

Table 1 Chemical composition of Ti45Nb alloy

Element	wt%	wt% error	at. %	at. % error
Ti	53.92	± 0.81	69.22	± 1.04
V	0.51	± 0.46	0.62	± 0.55
Nb	45.57	± 0.83	30.16	± 0.55

Table 2 Parameters of different stages of hydrostatic extrusion

Sample names	Staged	Initial dia (mm)	Final dia (mm)	Reduction factor (Area)	Accumulative reduction factor	True strain	Accumulative true strain	Pressure (MPa)
HE15	1st	30	15	4	4	1.38	1.38	565
HE10	2nd	14.5	10	2.1	8.4	0.74	2.12	704
HE8	3rd	10	8	1.56	13.1	0.44	2.57	843
HE7	4th	8	7	1.3	17	0.26	2.83	791
HE6	5th	7	6	1.36	23.2	0.31	3.14	750
HE5	6th	6	5	1.44	33.4	0.36	3.2	825

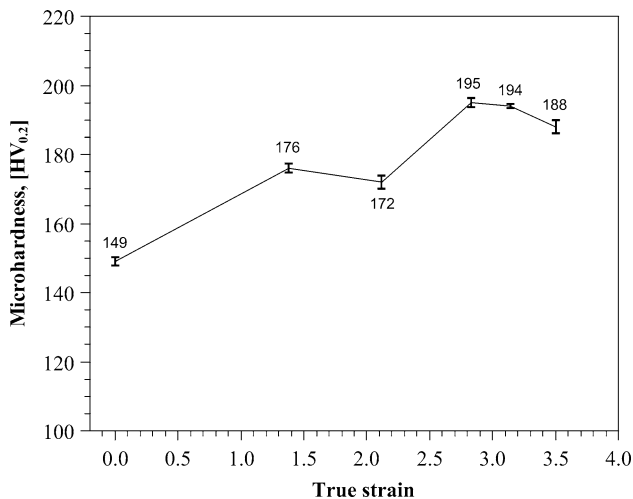
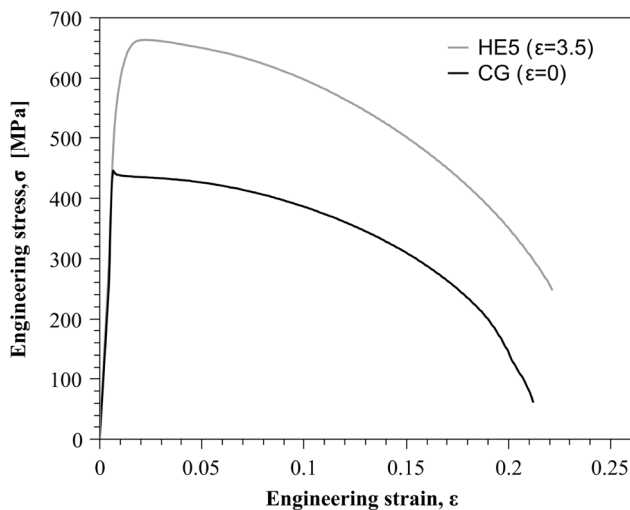
**Fig. 1** Microhardness as a function of true strain**Fig. 2** Stress–strain curves of materials CG and HE5

Figure 2 shows the stress–strain curves of CG and HE5 specimens obtained by micro-tensile tests. The ultimate tensile strength increased by 50 % from 445 to 663 MPa

and yield stress increased by 45 % from 430 to 620 MPa. It is worth noting that the fracture strain of HE5 sample has only slightly changed from 23 to 21.7 %, despite the fact that SPD materials generally exhibit reduced ductility [37]. This is a favourable characteristic for metals intended for orthopaedic applications.

Figure 3 shows load versus displacement curves and the changes in Young's modulus during the consecutive HE processing steps. The values of Young's modulus measured with the highest HE deformation did not exceed 68.8 GPa which is only slightly higher than 62.7 GPa measured for the CG samples. This increase corresponds to about 9 % only, and thus fulfils the requirement that any strengthening procedure in Ti–Nb biomedical alloy should not increase the Young's modulus too much in order to avoid the stress shielding effect and thus the gradual deterioration of bone material, as it may occur with conventional α -type titanium alloys having a Young's modulus of about 110 GPa. It should be noted that Matsumoto et al. [38] reported for another β -type alloy (Ti–35Nb–4Sn) that Young's modulus decreases as a function of strain applied in cold rolling. This was attributed to the transformation of β -phase to orthorhombic α'' one. The alloy investigated in the present study has higher Nb content, which not only stabilizes β -phase but also facilitates β to ω transformation, as reported and discussed within this paper later on. Such a transformation may result in an increase of Young's modulus, since ω -phase is stiffer than the β one.

In order to maintain the Young's modulus at a relatively low level typical of β -Ti alloys, it is essential to avoid any phase transformation during processing. Figure 4 shows XRD patterns of all samples before and after different strains of HE. The results show that all peaks correspond to the β -phase, which suggests that no phase transformation takes place during HE processing. The variations in the peak intensity can be attributed to the changes in crystallographic texture, which is a consequence of the HE process. One could also argue that these changes in texture cause the variations in microhardness and/or Young's modulus shown in Figs. 1 and 3b, respectively. However, two facts speak against this suspicion: (i) Vickers

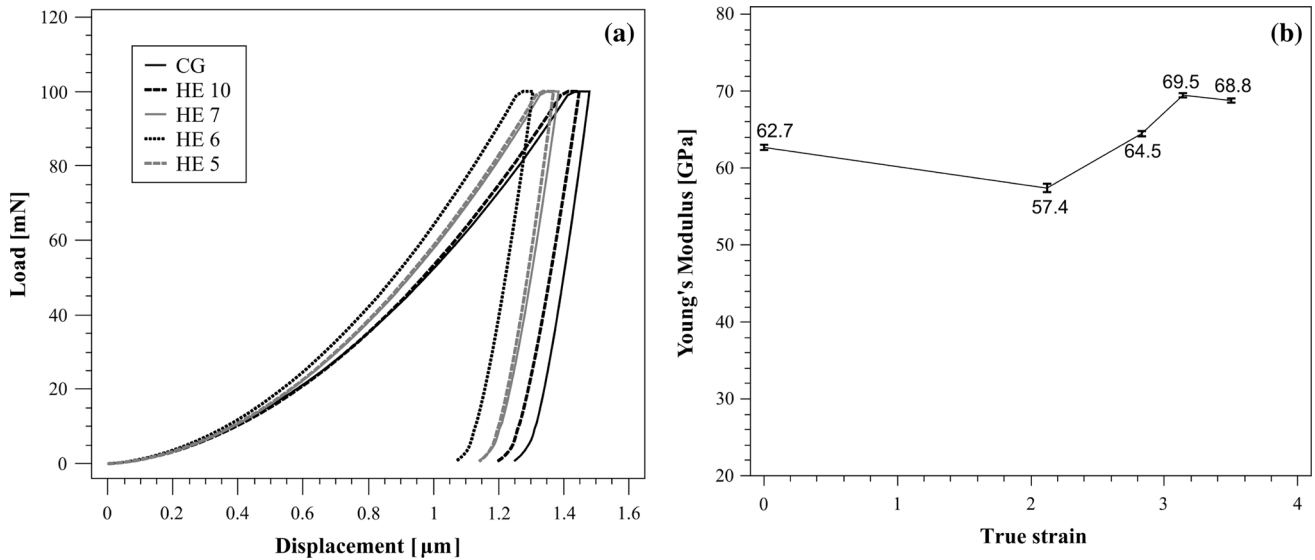


Fig. 3 Nanoindentation results of CG and HE-processed samples: **a** load versus displacement curves and **b** Young's modulus values

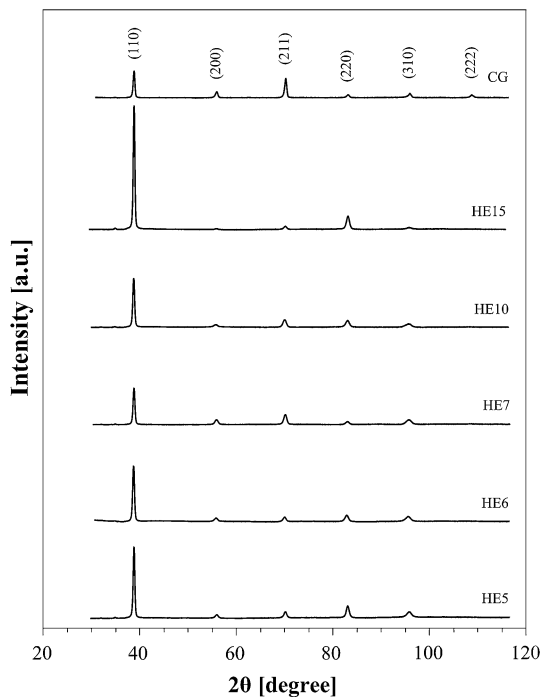


Fig. 4 X-ray diffraction pattern of the samples after each stage of HE

microhardness is known to be not too sensitive to lattice orientation and thus to texture changes; (ii) calculations of changes in Young's modulus according to texture changes cannot reflect the experimental data, according to recent investigations which will be published elsewhere [39].

The microstructure of the CG sample as inspected by optical microscopy consists of equiaxed β -grains with an average grain size of 23 μm , as illustrated in Fig. 5a. HE

processing brings about a significant microstructure refinement (Fig. 5b). However, the microstructure after HE is quite heterogeneous and, as illustrated in Fig. 6, some typical regions can be distinguished.

The first typical region consists of relatively small elongated grains, as shown in Fig. 6a. The diffraction pattern in the form of rings suggests different orientations of individual grains, and the presence of high-angle grain boundaries between them. The average grain size was found to be about 300 nm. This region seems to be the most advanced stage of grain refinement reported in this study. Inside the small grains, the density of dislocations is relatively high, but they are not arranged in special substructures. The amplitude contrast changes within some grains which can be attributed to the existence of residual stresses.

The remaining microstructure shows a deformation substructure. It consists of relatively large grains with $\langle 011 \rangle$ direction parallel to the extrusion direction (the diffraction pattern was taken at zero tilt). Inside the grains, low-angle grain boundaries are present (Fig. 6b) and some deformation twins with habit plane of $\{121\}$ typical for bcc metals (Fig. 6c) can be recognized.

As the microstructure exhibits different types of substructures, each of them will give different reactions to applied stress. High-angle grain boundaries and mechanical twins seem to act as obstacles to dislocation motion causing a strengthening effect [40, 41]. However, the presence of relatively large grains with dislocations and low-angle grain boundaries indicate that the material can even accumulate more strain [42], so that it allows applying further HE stages based on the same requirements. The

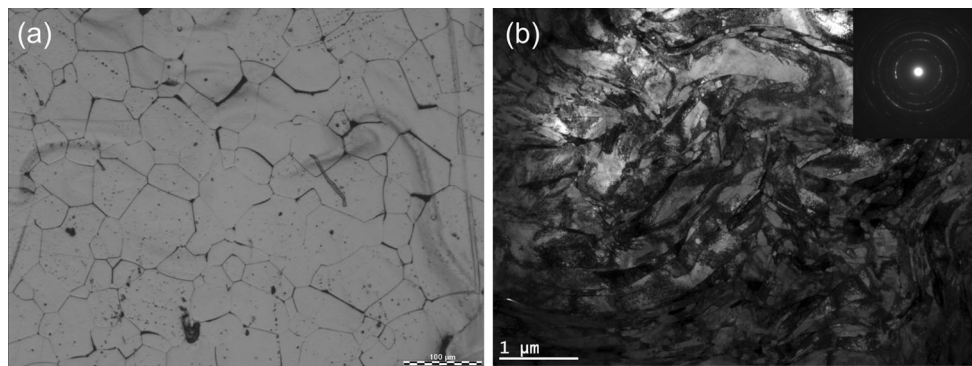


Fig. 5 General view of microstructure of Ti-45Nb: **a** CG and **b** HE5 samples

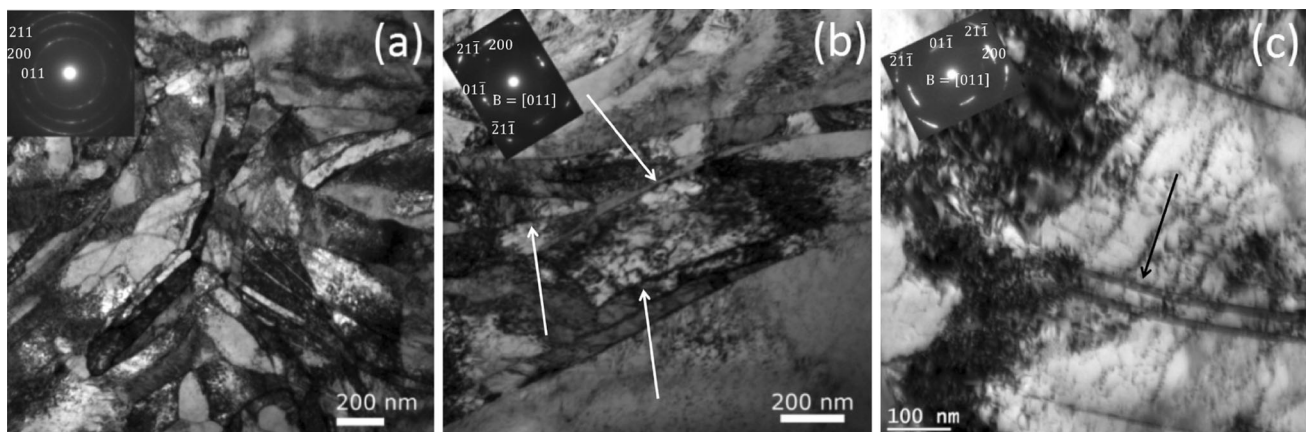


Fig. 6 Images of different areas in HE5 specimens extruded with a true strain of 3.5: **a** small grains, **b** elongated grains with relatively large dimensions and **c** a typical grain representing dislocation

co-existence of small and large grains allows for both enhancement of strength and almost stable strain [43]. This can explain why the values of fracture strain observed for both CG and UFG specimens are almost identical.

Compared to CP-Ti (HE processed at ambient temperature with a total true strain of 3.77) examined by Topolski et al. [44], the improvement of mechanical strength by HE in Ti-45Nb is lower (Figs. 1, 2). In the case of CP-Ti, the improvements were between 110 % (ultimate tensile strength) and about 250 % (yield strength).

The reason of the different efficiency of HE in terms of strengthening in those materials can be attributed to less advanced process of grain refinement in the Ti-45Nb alloy. In the case of CP-Ti, a homogeneous microstructure with an average grain size of 55 nm was obtained, while for the current β -type titanium alloy, only a fraction of microstructure exhibited grains with sizes below 1 μm . The different potentials for grain refinement can be attributed to different mechanisms of plastic deformation taking place in hcp (α) and bcc (β) titanium. In α -Ti, grain refinement occurs via the combination of various twinning modes and dislocation glide [45]. Detailed studies were done for different ECAP routes and have shown that the final

substructure and twins. The images are orientated perpendicularly to the extrusion direction. *White* and *black arrows* indicate low-angle grain boundaries and twins, respectively

microstructure strongly depends on the number of active slip systems induced by stress conditions defined by deformation route. Such an analysis has not been done for β -Ti. However, deformation in bcc metals is expected to be significantly different from deformation in hcp metals since the close-packed direction $\langle 111 \rangle$ belongs to many planes in contrast to the hcp case. As a result, the formation of dislocation jogs in bcc lattice structure occurs rarely compared to the hcp lattice [42], and the grain refinement is less advanced.

Careful inspection of the microstructure revealed in some places a zig-zag structure (Fig. 7), which can be described as a combination of ω -phase with deformation twins caused by shearing [46]. Diffraction pattern presented as an inset displays diffusive lines between spots of (200) and (110) planes in [011] zone axis pattern. Such lines may be caused by scattering by ω -phase as reported by Yano et al. [47]. The presence of small amount of ω -phase can explain the observed variations in Young's modulus in HE-processed samples as Young's modulus of ω -phase is higher than that of β -phase [48, 49]. However, this will be a subject of more detailed investigation in near future.

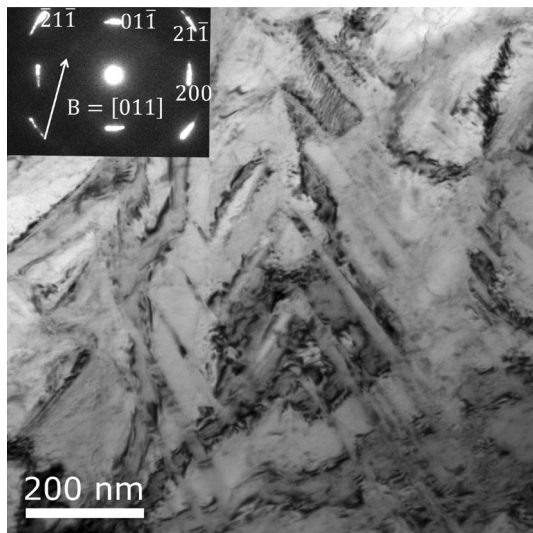


Fig. 7 TEM image of a zig-zag structure in HE5 sample (extruded to a true strain of 3.5), diffused spots from ω -phase are indicated by an arrow

Conclusions

In the present study, it has been shown that HE is an efficient technique in tailoring mechanical properties of β -type Ti–Nb alloy. The strength was significantly improved by 45 % due to grain boundary and dislocation strengthening mechanisms. The Young's modulus was kept at a low level (below 70 GPa), thanks to maintaining almost a single-phase β -structure during HE processing. Furthermore, HE processing did not deteriorate plasticity of high-strength material which can be attributed to the presence of large grains, which still have ability to accommodate plastic deformation during further straining.

Acknowledgements This work was supported within the EU 7th framework programme FP7/2007–13 under Marie-Curie project Grant No. 264635 (BioTiNet-ITN).

Open Access This article is distributed under the terms of the Creative Commons Attribution License which permits any use, distribution, and reproduction in any medium, provided the original author(s) and the source are credited.

References

- Calin M, Gebert A, Ghinea AC, Gostin PF, Abdi S, Mickel C, Eckert J (2013) Designing biocompatible Ti-based metallic glasses for implant applications. *Mater Sci Eng C* 33:875–883
- Godley R, Starosvetsky D, Gotman I (2006) Corrosion behavior of a low modulus β -Ti–45% Nb alloy for use in medical implants. *J Mater Sci Mater Med* 17:63–67
- Kuroda D, Niinomi M, Morigana M, Kato Y, Yashiro T (1998) Design and mechanical properties of new β type titanium alloys for implant materials. *Mater Sci Eng A* 243:244–249
- Purcek G, Saray O, Karaman I, Yapici GG, Haouaoui M, Maier HJ (2009) Mechanical and wear properties of ultrafine-grained pure Ti produced by multi-pass equal-channel angular extrusion. *Mater Sci Eng A* 517:97–104
- Hon YH, Wang JY, Pan YN (2003) Composition/phase structure and properties of titanium–niobium alloys. *Mater Trans* 41: 2384–2390
- Martins GV, Silva CRM, Nunes CA, Trava-Airoldi VJ, Borges JLA, Machado JPB (2010) Beta Ti–45Nb and Ti–50Nb alloys produced by powder metallurgy for aerospace application. *Mater Sci Forum* 660–661:405–409
- Bauer S, Schmuki P, Mark KVD, Park J (2013) Progress in materials science engineering biocompatible implant surfaces part I : materials and surfaces. *Prog Mater Sci* 58:261–326
- Gostin PF, Helth A, Voss A, Sueptitz R, Calin M, Eckert J, Gebert A (2013) Surface treatment, corrosion behavior, and apatite-forming ability of Ti–45Nb implant alloy. *J Biomed Mater Res Part B* 101B:269–278
- Nakai M, Niinomi M, Hieda J, Yilmazer H, Tokada Y (2013) Heterogeneous grain refinement of biomedical Ti–29Nb–13Ta–4.6Zr alloy through high-pressure torsion. *Sci Iran F* 20: 1067–1070
- Williams JC, Lutjering G (2007) Titanium, 2nd edn. Springer, New York
- Niinomi M (2008) Review: mechanical biocompatibilities of titanium alloys for biomedical applications. *J Mech Behav Biomed* 1:30–42
- Gepreel MAH, Niinomi M (2013) Biocompatibility of Ti-alloys for long-term implantation. *J Mech Behav Biomed* 20:407–415
- Niinomi M (1998) Mechanical properties of biomedical titanium alloys. *Mater Sci Eng A* 243:231–236
- Yilmazer H, Niinomi M, Nakai M, Cho K, Hieda J, Todaka Y, Miyazaki T (2013) Mechanical properties of a medical β -type titanium alloy with specific microstructural evolution through high-pressure torsion. *Mater Sci Eng C* 33:2499–2507
- Valiev RZ, Gunderov DV, Lukyanov AV, Pushin VG (2012) Mechanical behaviour of nanocrystalline TiNi alloy produced by severe plastic deformation. *J Mater Sci* 47:7848–7853. doi:10.1007/s10853-012-6579-8
- Sordi VL, Ferrante M, Kawasaki M, Langdon TG (2012) Microstructure and tensile strength of grade 2 titanium processed by equal-channel angular pressing and by rolling. *J Mater Sci* 47:7870–7876. doi:10.1007/s10853-012-6593-x
- Saitova LR, Hoppel HW, Goken M, Semenova IP, Raab GI, Valiev RZ (2009) Fatigue behavior of ultrafine-grained Ti–6Al–4 V ‘ELI’ alloy for medical applications. *Mater Sci Eng A* 503:145–147
- Valiev RZ, Islamgaliev RK, Alexandrov IV (2000) Bulk nanostructured materials from severe plastic deformation. *Prog Mater Sci* 45:103–189
- Pippan R (2009) High pressure torsion—features and applications. In: Zehetbauer MJ, Zhu YT (eds) Bulk nanostructured materials. Wiley, Weinheim, p 217
- Estrin Y, Vinogradov A (2010) Fatigue behaviour of light alloys with ultrafine grain structure produced by severe plastic deformation: an overview. *Int J Fatigue* 32:898–907
- Lewandowska M, Kurzydowski KJ (2005) Thermal stability of a nanostructured aluminium alloy. *Mater Charact* 55:395–401
- Kulczyk M, Pachla W, Mazur A, Sus-Ryszkowska M, Krasilnikov N, Kurzydowski KJ (2007) Producing bulk nanocrystalline materials by combined hydrostatic extrusion and equal-channel angular pressing. *Mater Sci Pol* 25:991–999
- Chen Y, Li J, Tang B, Kou H, Zhang F, Chang H, Zhou L (2013) Grain boundary character distribution and texture evolution in cold-drawn Ti–45Nb wires. *Mater Lett* 98:254–257

24. Park CH, Park JW, Yeom JT, Chun YS, Lee CS (2010) Enhanced mechanical compatibility of submicrocrystalline Ti–13Nb–13Zr alloy. *Mater Sci Eng A* 527:4914–4919
25. Zherebtsov S, Lojkowski W, Mazur A, Salishchev G (2010) Structure and properties of hydrostatically extruded commercially pure titanium. *Mater Sci Eng A* 527:5596–5603
26. Zherebtsov S, Mazur A, Salishchev G, Lojkowski W (2008) Effect of hydrostatic extrusion at 600–700 °C on the structure and properties of Ti–6Al–4 V alloy. *Mater Sci Eng A* 485:39–45
27. Zherebtsov S, Salishchev G, Lojkowski W (2009) Strengthening of a Ti–6Al–4 V titanium alloy by means of hydrostatic extrusion and other methods. *Mater Sci Eng A* 515:43–48
28. Lewandowska M, Kurzydowski KJ (2008) Recent development in grain refinement by hydrostatic extrusion. *J Mater Sci* 43:7299–7306. doi:10.1007/s10853-008-2810-z
29. Pachla W, Kulczyk M, Swiderska-Sroda A, Lewandowska M, Garbacz H, Mazur A, Kurzydowski KJ (2006) Nanostructuring of metals by hydrostatic extrusion. *Proc Int Esaform Conf Mater Form* 16:535–538
30. Lewandowska M, Wawer K (2007) Optimization of particle size and distribution by hydrostatic extrusion. *Mater Sci Forum* 561–565:869–872
31. Pakielka Z, Garbacz H, Lewandowska M, Druzycka-Wienciek A, Sus-Ryszkowska M, Zielinski W, Kurzydowski KJ (2006) Structure and properties of nanomaterials produced by severe plastic deformation. *Nukleonika* 51:19–25
32. Pachla W, Kulczyk M, Sus-Ryszkowska M, Mazur A, Kurzydowski KJ (2008) Nanocrystalline titanium produced by hydrostatic extrusion. *J Mater Process Technol* 205:173–182
33. Oliver WC, Pharr GM (2004) Review: measurement of hardness and elastic modulus by instrumented indentation: advances in understanding and refinements to methodology. *J Mater Res* 19:3–20
34. Zehetbauer M, Trattner D (1987) Effects of stress aided static recovery in iteratively cold-worked aluminium and copper. *Mater Sci Eng* 89:93–101
35. Schafler E (2010) Effects of releasing the hydrostatic pressure on the nanostructure after severe plastic deformation of Cu. *Scr Mater* 62:423–426
36. Schafler E (2011) Strength response upon pressure release after high pressure torsion deformation. *Scr Mater* 64:130–132
37. Zehetbauer MJ, Valiev RZ (2004) *Nanomaterials by severe plastic deformation*. Wiley, Weinheim
38. Matsumoto H, Watanabe S, Hanada S (2007) Microstructures and mechanical properties of metastable β TiNbSn alloys cold rolled and heat treated. *J Alloys Compd* 439:146–155
39. Panigrahi A, Sulkowski B, Ozaltin K, Horky J, Lewandowska M, Waitz T, Skrotzki W, Zehetbauer M (2014) Mechanical properties and texture evolution in biocompatible Ti–45Nb alloy processed by severe plastic deformation (unpublished)
40. Hall EO (1951) The deformation and ageing of mild steel: III discussion of results. *Proc Phys Soc B* 64:747–753
41. Petch NJ (1953) The cleavage strength of polycrystals. *J Iron Steel Inst* 174:25–28
42. Kuhlmann-Wilsdorf D (1989) Theory of plastic deformation: properties of low energy dislocation structures. *Mater Sci Eng A* 113:1–41
43. Estrin Y, Vinogradov A (2013) Extreme grain refinement by severe plastic deformation: a wealth of challenging science. *Acta Mater* 61:782–817
44. Topolski K, Garbacz H, Kurzydowski KJ (2008) Nanocrystalline titanium rods processed by hydrostatic extrusion. *Mater Sci Forum* 584–586:777–782
45. Shin DH, Kim I, Kim J, Kim YS, Semiatin SL (2003) Microstructure development during equal-channel angular pressing of titanium. *Acta Mater* 51:983–996
46. Xing H, Sun J (2008) Mechanical twinning and omega transition by $\langle 111 \rangle \{112\}$ shear in a metastable β titanium alloy. *Appl Phys Lett* 93:031908
47. Yano T, Murakami Y, Shindo D, Hayasaka Y, Kuramoto S (2010) Transmission electron microscopy studies on nanometer-sized ω phase produced in gum metal. *Scr Mater* 63:536–539
48. Tane M, Nakano T, Kuramoto S, Niinomi M, Takesue N, Nakajima H (2013) ω transformation in cold-worked Ti–Nb–Ta–Zr–O alloys with low body-centered cubic phase stability and its correlation with their elastic properties. *Acta Mater* 61:139–150
49. Banerjee D, Williams JC (2013) Perspectives on titanium science and technology. *Acta Mater* 61:844–879